AD-A176 325 STRUCTURE AND PROPERTIES OF POLYMER INTERPHASES(U) 1/1
CINCINNATI UNIV OH DEPT OF MATERIALS SCIENCE AND
ENGINEERING F J BOERIO 01 DEC 86 N00014-85-K-0459
UNCLASSIFIED F/G 11/1 NL

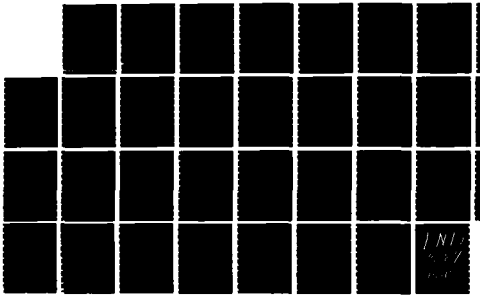

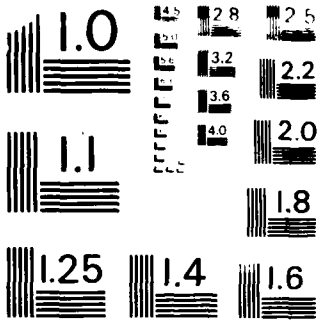

MICROCOPY RESOLUTION TEST CHART

(12)

Annual Report No. 1
Contract N00014-85-K-0459; NR-4313-202

Structure and Properties of Polymer Interphases

F. James Boerio
Department of Materials Science and Engineering
University of Cincinnati
Cincinnati, Ohio 45221

December 1, 1986

Interim Report for Period July 1, 1985 to June 30, 1986

Prepared for:

Office of Naval Research
800 North Quincy Street
Arlington, VA 22217

SECURITY CLASSIFICATION OF THIS PAGE

AD-A176325

REPORT DOCUMENTATION PAGE

1a. REPORT SECURITY CLASSIFICATION	1b. RESTRICTIVE MARKINGS
2a. SECURITY CLASSIFICATION AUTHORITY	3. DISTRIBUTION / AVAILABILITY OF REPORT: Unlimited
2b. DECLASSIFICATION / DOWNGRADING SCHEDULE	
4. PERFORMING ORGANIZATION REPORT NUMBE (S): Annual Report No. 1	5. MONITORING ORGANIZATION REPORT NUMBER(S)
6a. NAME OF PERFORMING ORGANIZATION: University of Cincinnati; 6b. OFFICE SYMBOL (If applicable)	7a. NAME OF MONITORING ORGANIZATION: Office of Naval Research Resident Representative
6c. ADDRESS (City, State, and ZIP Code): Department of Materials Science and Engineering, Cincinnati, OH 45221-0012	7b. ADDRESS (City, State, and ZIP Code): 1314 Kinnear Road, Columbus, OH 43212
8a. NAME OF FUNDING SPONSORING ORGANIZATION: Office of Naval Research; 8b. OFFICE SYMBOL (If applicable): N00014	9. PROCUREMENT INSTRUMENT IDENTIFICATION NUMBER: N00014-85-R-0459
8c. ADDRESS (City, State, and ZIP Code): 800 North Quincy Street, Arlington, VA 22217-5000	10. SOURCE OF FUNDING NUMBERS: PROGRAM ELEMENT NO; PROJECT NO; TASK NO; WORK UNIT ACCESSION NO: NR-4313-202

11. TITLE (Include Security Classification): Structure and Properties of Polymer Interphases

12. PERSONAL AUTHOR(S): F. James Boerio

13a. TYPE OF REPORT	13b. TIME COVERED	14. DATE OF REPORT (Year, Month, Day)	15. PAGE COUNT
Interim	FROM 7/1/85 TO 6/30/86	December 1, 1986	47

16. SUPPLEMENTARY NOTATION

17. COSATI CODES			18. SUBJECT TERMS (Continue on reverse if necessary and identify by block number)
FIELD	GROUP	SUB-GROUP	

19. ABSTRACT (Continue on reverse if necessary and identify by block number)

The structure of polymer interphases in adhesive joints has been determined using x-ray photoelectron spectroscopy and internal reflection infrared spectroscopy. When an epoxy adhesive was cured against 2024 aluminum using a polyamine curing agent, the amount of crosslinking in the adhesive adjacent to the oxide was significantly higher than in the bulk adhesive due to catalysis of the curing reaction by hydroxyl groups present on the oxidized surface of the aluminum and to protonation of the amino groups on the polyamine curing agent.

When an epoxy adhesive was cured against titanium that had been pre-treated with dilute aqueous solutions of γ-aminopropyltriethoxysilane (γ-APS), the structure of the interphase depended on the curing agent. With tertiary amine salt curing agents, there was little interdiffusion of

20. DISTRIBUTION / AVAILABILITY OF ABSTRACT: ☐ UNCLASSIFIED/UNLIMITED ☐ SAME AS RPT ☐ DTIC USERS	21. ABSTRACT SECURITY CLASSIFICATION
22a. NAME OF RESPONSIBLE INDIVIDUAL	22b. TELEPHONE (Include Area Code) / 22c. OFFICE SYMBOL

DD FORM 1473, 84 MAR — 83 APR edition may be used until exhausted. All other editions are obsolete.

SECURITY CLASSIFICATION OF THIS PAGE

ABSTRACT (cont'd.)

the silane and the epoxy and the interphase consisted mostly of a siloxane polymer. However, when anhydride curing agents were used, there was considerable interdiffusion of the silane and the epoxy and the silane reacted with the curing agent to form an interphase that contained amide and a few imide groups.

Metal substrates were found to have a significant effect on the structure of the silane primer. When γ-APS films were deposited on iron or titanium and then dried at 110°C, the silane polymerized to form high molecular weight siloxane polymers. The amino groups in the siloxane polymers absorbed carbon dioxide and water from the atmosphere to form amine bicarbonate salts. However, when similar films were deposited on 2024 aluminum or copper and then dried, polymerization of the silane was inhibited and the amino groups were oxidized to form imine groups.

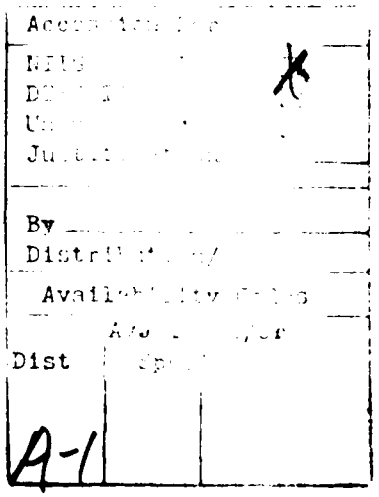

I. Introduction

A great deal of progress has been made in recent years in modifying interfaces in adhesive joints and composites for improved stability in aggressive environments. For example, aluminum has frequently been prepared for adhesive bonding by etching in an aqueous solution of chromic and sulfuric acids (the FPL etching process). This process produced an oxide that was very porous and enabled the formation of strong adhesive bonds to aluminum substrates in dry environments (1). However, the oxide had poor corrosion resistance and the adhesive bonds had poor durability during exposure to moist environments (2).

Very recently it has been shown that anodizing aluminum in phosphoric acid produces a porous oxide (1) that has very good corrosion resistance (2). Strong, stable adhesive bonds may be obtained with aluminum adherends that have been anodized in phosphoric acid. Somewhat similar results have been obtained for titanium. Anodizing titanium in chromic acid provides a rather porous, stable oxide that enables the formation of strong, durable bonds to titanium substrates (3).

It is well known that the poor hydrothermal stability of adhesive bonds to aluminum is related to hydration of the oxide (4). The outstanding hydrothermal stability of the oxide obtained by anodizing aluminum in phosphoric acid has been attributed to the formation of a monomolecular layer of $AlPO_4$ on the surface of the oxide (4). This compound has

very low solubility in water and inhibits hydration of the oxide. Similar hydration inhibitors, such as nitrilotris-methylenetriphosphonic acid (NTMP), can be used to improve the stability of the oxide produced on aluminum by the FPL etching process (5).

Surface pretreatment can also be used to obtain improved performance in graphite-reinforced composites. Oxidation of graphite fibers improves the fiber/matrix shear strength by removing a weak layer from the fiber surfaces and by introducing reactive oxygen atoms into the surfaces (6).

Organofunctional silane "coupling agents" have been used to improve the hydrothermal stability of glass fiber reinforced composites. We showed that thin films of silanes such as γ-aminopropyltriethoxysilane (γ-APS) are extremely effective primers for improving the hydrothermal stability of iron/epoxy adhesive joints (7,8). γ-APS was also an effective primer for titanium/epoxy adhesive joints (7) but there were some differences between the performance of γ-APS on iron and on titanium. γ-APS is usually applied from dilute aqueous solutions and the pH of the solutions was a very important variable for iron substrates but was less important for titanium. Very recently we have shown that γ-APS is also an effective primer for enhancing the hydrothermal stability of aluminum/epoxy adhesive bonds (9).

Considerable progress has also been made in developing analytical techniques for determining the chemical and

physical structures of surfaces. Vacuum techniques, such as Auger electron spectroscopy (AES) and x-ray photoelectron spectroscopy (XPS), have been useful for characterizing pretreated substrates and failure surfaces (10). Optical techniques such as infrared spectroscopy, especially Fourier transform infrared spectroscopy (FTIR), have been particularly useful in characterizing thin films such as primers and oxides formed on metals (11).

There has been a great deal of progress in modifying polymer interfaces so as to obtain improved performance in adhesive joints and composites. Significant progress has also been made in characterizing the surface regions of solids. However, there are some areas relevant to adhesive bonding and composites where few advances have been made. Those areas include determining the structure of polymer interphases and developing analytical techniques for the in situ, non-destructive determination of the stability of polymer interfaces during exposure to aggressive environments.

In this report, initial results from our investigation of polymer interphases are described. Subsequent reports will also describe the use of ellipsometry as a continuous, in-situ, non-destructive technique for determining the stability of polymer interfaces during exposure to harsh environments.

Interphases represent the transition regions between polymer/substrate interfaces and the bulk of the polymer.

As a first approximation, it is usually assumed that the properties of the interphase are the same as those of the bulk polymer. However, chemical and physical processes are influenced by interfaces and there may be a gradation or properties as the interface is approached. For example, the presence of the interface and the nature of the interface may cause orientation effects within the polymer or changes in the curing reactions of the polymer. However, the extent of these structural gradations and their depth away from the interface and into the polymer are not well known.

We are using analytical techniques such as internal reflection or attenuated total reflection infrared spectroscopy (ATR), x-ray photoelectron spectroscopy (XPS), and external reflection or reflection-absorption infrared spectroscopy (RAIR) to determine the structure of polymer interphases. All of these techniques have been described in the literature. As a result, only some of the most important features of each will be discussed here.

XPS is a non-destructive, highly surface-sensitive technique for determining the composition of the outermost few tens of angstroms of a solid. When the surface of a solid is irradiated with x-rays, core level electrons can be ejected from atoms near the surface if the energy of the x-rays is greater than the sum of the electron binding energy and the work function of the spectrometer .

Since energy is conserved in this process, the binding energies of the photoelectrons can be obtained from the expression

$$T = h\upsilon - E_b - (\phi)$$

where T is the kinetic energy of the ejected electron, $h\upsilon$ is the energy of the incident photon, E_b is the binding energy of the electron, and ϕ is the work function of the spectrometer. Since the binding energies of the electrons in each element are unique, the composition of a solid can be determined from measurements of the binding energies of the emitted photoelectrons. Moreover, changes in the oxidation state of an atom result in small changes in the binding energies, making it possible to obtain some information about the chemical bonding in the solid.

XPS is very surface-sensitive even though electrons are emitted from deep within the solid. That is because the probability of an electron escaping from the solid without losing energy in inelastic collisions is a function of the material, the kinetic energy of the electron, and the depth beneath the surface from which the photoelectron originated. The depth below which less than 1/e of the emitted electrons of a given energy escape the solid without having undergone inelastic collisions is termed the escape depth and represents the depth of material that is responsible for most of the intensity of a photoelectron peak. The escape depth for organic solids is typically a few tens of angstroms (12).

One valuable aspect of XPS is the ability to do non-destructive depth profiling by varying the "exit angle," the angle between the solid surface and the optical axis of the electron energy analyzer (see Figure 1). The analysis depth, x, is related to the escape depth, d, by the expression

$$x = d \sin(\theta) \qquad (1)$$

where θ is the exit angle. When the sample surface is normal to the optical axis of the analyzer (Figure 1A), the escape depth and the analysis depth are equal. However, when the exit angle is decreased (Figure 1B), the analysis depth decreases and a larger percentage of the detected electrons will have originated from near the surface.

Another interesting aspect of XPS concerns surface morphology (13). When XPS data are obtained from a surface at several exit angles, it is possible to distinguish between several different morphologies. For the model substrate/overlayer surface structures shown in Figure 2A, the equations governing signal intensity are as follows:

$$I_s = f(\theta)\ I_s(\infty)\ \exp(-d/\lambda_s \sin\ ) \qquad (2)$$

$$I_o = f(\theta)\ I_o(\infty)\ (1-\exp(-d/\lambda_o \sin\ ) \qquad (3)$$

Where I_s is the intensity for electrons originating in the substrate, I_o is the intensity for electrons originating in the overlayer, $f(\theta)$ is the spectrometer sensitivity as a function of exit angle, $I_s(\infty)$ is the intensity in the absence of an overlayer, $I_o(\infty)$ is the intensity when the overlayer is "infinitely" thick, d is the thickness of the

overlayer, λ is the escape depth of photoelectrons, and θ is the angle between the optical axis of the electron energy analyzer and the sample surface.

Equation 2 shows that the intensity of the signal arising from the substrate increases exponentially as the angle between the electron energy analyzer and the sample surface is increased. Equation 3 shows that the intensity of signals arising from species in the overlayer decrease in a similar exponential manner as the spectrometer exit angle is increased.

Other surface morphologies can be identified by the functional dependence of intensity on exit angle (13,14). If the surface phase is present as a discontinuous film whose thickness is less than the electron escape depth (Figure 2B), then the intensity of the surface phase will again show an exponential dependence on exit angle as described by equation 2. However, both substrate and overlayer species will be present at the surface in this instance, and the intensity of bands arising from species in the bulk or substrate phase will not show as strong a dependence on exit angle as predicted by equation 3.

If the surface phase is present as a discontinuous film whose average thickness is greater than the electron escape depth (Figure 2C), then both phases will again be visible at all exit angles. The intensity of peaks arising from material in the surface phase will not, however, show a dependence on spectrometer exit angle.

Internal reflection or ATR infrared spectroscopy is an extremely useful technique for determining the composition of the surface regions of polymers (15). In ATR, the surface of a polymer is pressed against the surface of a transparent crystal (internal reflection element) with a refractive index greater than that of the polymer and infrared radiation is directed at the interface from within the crystal (see Figure 3). If the angle of incidence is greater than some critical angle and the polymer is not absorbing, total reflection of the radiation back into the crystal will occur at the interface. An electric field will still exist within the polymer but it will not propagate and its amplitude will decay exponentially with distance into the polymer. When the frequency of the infrared radiation equals that of a vibrational mode in the polymer, energy will be absorbed by the polymer and the reflectivity of the interface will decrease. Thus, an attenuated total reflection (ATR) infrared spectrum can be obtained from the polymer by varying the frequency of the infrared radiation.

The amplitude of the electric field in the polymer will decrease to 1/e of its value at the interface at a distance δ into the polymer. δ is referred to as the penetration depth (15) of the radiation in the polymer and is given by the expression

$$\delta = \lambda_o/(2\pi n_2((n_1/n_2)^2 \sin^2\theta - 1)^{1/2}) \qquad (4)$$

where λ_o is the wavelength of the radiation in vacuum, n_1 and n_2 are the refractive indices of the crystal and the

polymer, and θ is the angle of incidence. Depth profiling can be accomplished by changing δ. Equation 4 shows that δ can be increased by decreasing the angle of incidence or the refractive index of the crystal. However, δ is several thousand angstroms for most polymer/crystal combinations and ATR is not as surface sensitive as XPS.

RAIR is a technique for obtaining the infrared spectra of extremely thin films on reflecting substrates by reflecting infrared radiation that is polarized parallel to the plane of incidence off of the surface at large, grazing angles of incidence (11). Under these conditions, the incident and reflected waves combine to form a standing wave that has considerable amplitude at the surface. On good reflectors such as polished or evaporated metals, RAIR allows useable spectra to be obtained from surface films approximately a monomolecular layer in thickness. Because the band size in a typical RAIR experiment is only a small percentage of the total reflected energy, FTIR spectrometers greatly facilitate the use of this technique by providing improved signal to noise ratios and greatly reduced scan time when compared to typical dispersive spectrophotometers.

In RAIR, the electric vector at the interface between the film and the substrate is perpendicular to the surface of the substrate. As a result, absorption bands due to vibrational modes polarized perpendicular to the surface appear with enhanced intensity when RAIR spectra are compared to transmission spectra but bands corresponding to

modes polarized parallel to the surface appear with reduced intensity. This feature makes RAIR very useful for determining the orientation of adsorbed species.

II. Experimental

The samples used in this investigation were double cantilever beams consisting of thick beams of adhesive cast onto polished aluminum and titanium beams. The geometry of these samples resulted in large residual stresses forming at the interface due to differential thermal contraction and polymerization shrinkage and allowed cracks to be easily propagated near the interface, exposing the interphase at the adhesive/substrate interface for examination.

The aluminum substrates consisted of beams of 2024-T3 alloy that were mechanically polished using standard metallographic techniques. The beams were initially degreased in acetone, washed with a mild detergent, and cleaned for five minutes in a mixture of sulfuric acid and sodium dichromate. Beams were polished with succesively finer grades of dry SiC paper and then polished with 14.5 micron alumina powder and MgO on Microcloth (Beuhler, Inc.), resulting in surfaces that were bright mirrors. Previous analysis of such surfaces using RAIR and XPS (16) showed that they consisted of a thin film (about 40 A) of amorphous Al_2O_3 and some hydroxide, probably pseudoboehmite, that contained both molecular water and water of hydration. The amount of hydrocarbon contamination present on the surfaces as determined by XPS and RAIR was quite small and the

surfaces were easily wetted by adhesives based on epoxy resins derived from the diglycydl ether of bisphenol-A epoxy (16).

The adhesive used with the aluminum substrates consisted of a low molecular weight DGEBA epoxy resin (Epon 828, Shell Chemical Co.) cured with 10 phr of triethylene-tetraamine (TETA, Fisher Scientific Co.). The resin was outgassed in a vacuum oven at 50°C and then combined with the curing agent in a beaker using a magnetic stirrer. Heating of the resin before addition of the curing agent facilitated complete mixing and reduced the viscosity, helping to ensure that complete wetting of the substrate was kinetically possible.

An aluminum mold, lined with 1/8" thick fluorocarbon plates, was clamped around the freshly prepared substrate and filled with the warm adhesive mixture. The samples were then allowed to cure overnight at room temperature, after which they were removed from the mold and postcured at 100°C for one hour. The resulting sample is shown in Figure 4.

After cooling from the postcure, residual stresses in the beams were high enough to cause visible deflection of the aluminum beam substrates. Interfacial cracks frequently started spontaneously, due to the magnitude of the stresses and the absence of mechanical interlocking with the polished surface, and were easily propagated by applying a light restoring force to the beams.

Preparation of samples with titanium substrates was very similar. Beams were machined from Ti-6Al, 4V alloy and then mechanically polished but 0.3 micron alumina was used in the final polishing. Two different adhesives were used with the titanium substrates. Both contained an epoxy resin (Epon 828) but one used a tertiary amine salt curing agent (K-61B, Pacific Anchor Chemical Co.) and the other used an anhydride curing agent (nadic methyl anhydride, Fisher Scientific Co.) with a tertiary amine accelerator (benzyl dimethylamine, Fisher). The adhesive with the tertiary amine salt curing agent was cured at 100^{o}C for one hour, removed from the mold, and post-cured at 150^{o}C for two hours. The adhesive with the anhydride curing agent was cured at 100^{o}C for two hours and then post-cured at 150^{o}C for two hours.

After the epoxy beams were debonded from the substrates, specimens for XPS and RAIR analysis were sectioned from both the adhesive and adherend failure surfaces using a band saw and spectra were obtained from the fracture surfaces as soon as possible, usually within minutes. XPS spectra were obtained using a Physical Electronics Model 5300 spectrometer using Mg K_{α} radiation at a power of 300 watts. All binding energies were referenced to the aliphatic C(1s) peak at 284.6 eV to correct for sample charging. The RAIR and ATR spectra were obtained using a Perkin-Elmer Model 1800 FTIR and reflection accessories from Harrick Scientific.

III. Results and Discussion

A. Interphase Composition in Aluminum/Epoxy Adhesive Joints

The Al(2p) XPS spectrum obtained from the epoxy fracture surface of an aluminum/epoxy double cantilever beam prepared using TETA as the curing agent is shown in Figure 5. A weak band related to aluminum was observed near 74.6 eV, indicating that crack propagation occurred at least in part through the oxide. The intensity of the band showed no dependence on the exit angle, suggesting that the aluminum was not present on the epoxy surface as a thin film, but as discrete particles whose thicknesses were greater than the escape depth of the photoelectrons.

The RAIR spectrum obtained from the corresponding aluminum fracture surface is shown in Figure 6. A weak band related to the epoxy resin was observed near 1510 cm^{-1}, indicating that a small amount of resin was retained on the aluminum surface. Electron microscopy of the aluminum fracture surfaces showed islands of a non-conducting material with dimensions on the order of microns which may have been cured resin. During crack propagation, the locus of failure apparently shifted between the epoxy resin and the aluminum oxide.

Analysis of the C(1s) XPS spectra of the fracture surfaces gave additional information as to the composition of the region in which failure took place. Figure 7A shows the curve-fit of the C(1s) spectrum obtained from a bulk specimen of cured epoxy. This specimen was fractured from

the interior of the cured beam and served as an example of the adhesive cured in the absence of an interface. The main component, located near 284.6 eV, was related to electrons from carbon atoms that were bonded only to hydrogen atoms or to other carbon atoms. The component shifted by 1.0 eV toward higher binding energy resulted from carbon atoms that were bonded to nitrogen atoms, while the component shifted upward by about 1.63 eV was characteristic of carbon atoms making single bonds to oxygen.

The curing reaction between epoxies and aliphatic amines results in the conversion of primary and secondary amines to secondary and tertiary amines as the amines open up the glycidyl ether rings through nucleophilic attack. Each of these cross-linking steps results in the formation of a CN bond at the expense of a CO bond. As the curing reaction proceeds there is an increase in the percentage of carbon atoms that are bonded to nitrogen atoms and a decrease in the percentage of carbon atoms that are bonded to oxygen atoms.

Table 1 shows the percentages of the different types of carbon atoms that were calculated for the bulk adhesive before and after cure. The percentages observed for the bulk cured resin and for the epoxy fracture surface are also shown. About 6.3% of the carbon atoms present in the uncured adhesive should exist in CN bonds. If the curing reaction proceeds so that all of the primary amines react to form tertiary amines, about 8.3% of all of the carbon should

exist in CN bonds. Analysis of the C(1s) spectra of the bulk cured resin (Figure 7A) showed that about 8.5% of the carbon atoms were bonded to nitrogen and that the reaction between TETA and DGEBA epoxies involves mostly the primary amines of the curing agent.

Figure 7B shows the C(1s) spectrum obtained from the epoxy fracture surface. Reference to Table 1 shows that the percentage of carbon atoms in CN and CO bonds was about 11.4% and 28%, respectively. However, atomic concentration measurements showed that the total amount of nitrogen and oxygen present on the fracture surface was about the same as in the bulk. This suggests that the degree of crosslinking in the interphase region is greater than in the material located farther away from the interface.

Additional information regarding the chemical composition of the interphase region was obtained from an examination of the N(1s) spectra of the resin and fracture surfaces. The N(1s) spectrum obtained from the bulk, cured material consisted of a strong component near 399 eV and a weak component about 1.6 eV toward higher energies that was about 3.2% of the total band area (see Figure 8A). When the N(1s) spectra from the epoxy and substrate sides of the fracture surface were examined, it was observed that the higher binding energy component increased in intensity to about 25% and 50% of the band area, respectively (see Figures 8B and 8C).

The band near 399 eV was related to nitrogen atoms bonded to hydrogen or carbon but the weak band at higher energies in the bulk epoxy was probably related to nitrogen atoms that were protonated by hydroxyl groups present in the cured DGEBA resin. The formation of amine hydrochlorides with residual HCl, a byproduct of the preparation of DGEBA resins, was considered as a possibility, but was ruled out because of the absence of any trace of chlorine in spectra of the cured resin. The formation of amine carbonates or bicarbonates with dissolved CO_2 was also considered, but the high-energy component was still observed in spectra obtained from cured adhesive prepared in an N_2 atmosphere from carefully degassed resin and curing agent.

Previous work using RAIR (16) has shown that the oxide present on the surface of mechanically polished 2024-T3 aluminum contains a large amount of hydroxide and molecular water. Isoelectric point measurements of these same surfaces (16) indicated that they are slightly acidic, with a pK_a between 7 and 4.5. It is likely that the higher binding energy nitrogen near the oxide surface resulted from protonation of amino nitrogen atoms in the curing agent by acidic hydroxyl groups on the as-polished surfaces.

Other work has also indicated that oxidized aluminum surfaces are able to protonate amines. XPS spectra of thin films of N-propylamine adsorbed onto polished 2024 aluminum showed the presence of high binding energy N(1s) electrons attributed to protonated amines (17). Also, angle-resolved

XPS of thin films of amino functional silanes deposited onto polished 2024 aluminum from dilute solution show high binding energy nitrogen material in the regions close to the oxide, and less high binding energy material farther away from the oxide surface (18).

As stated earlier, the aluminum present on the epoxy side of the fracture surface appeared to exist as island structures and not as a continuous film since the intensity of the Al(2p) peak did not change with exit angle. The high binding energy nitrogen material found on the epoxy side of the fracture surface and attributed to protonated amino groups also showed no dependence on exit angle. The demonstrated ability of the oxide to protonate amines suggests that the protonated amine compounds present on the adhesive failure surface near the interface were associated with the aluminum removed from the adherend surface during fracture. Most of the amines present on the aluminum fracture surface were in a region extremely close to the oxide surface, and therefore a larger percentage of the amines in this region were protonated.

Primary and secondary aliphatic amines act as initiators in the polymerization of epoxy resins. The amine nitrogen attaches to the terminal carbon atom of the epoxy ring in a nucleophilic addition reaction. This opens the epoxy ring and forms an oxygen anion from the glycidyl oxygen. Chain propagation occurs as the oxygen anions open other epoxy rings through nucleophilic addition. Both the initiation

and propagation steps require the presence of a proton donor to stabilize the intermediate oxygen anions (19,20).

The concentration of proton donors is a rate-limiting factor in the curing reaction (20). The concentration of material capable of functioning in this proton-donating role is low in the bulk resin and limited to the alcohol groups that are part of higher molecular weight DGEBA molecules and possibly to other stray molecules such as water or other impurities.

Proton donators are abundant, however, near the hydroxyl-rich aluminum oxide surface. This is suggested by the presence of protonated amino nitrogens in the vicinity of the aluminum oxide. These same hydroxyls are probably capable of catalyzing the curing reaction and are therefore probably responsible for the large amount of chain initiation steps detected in these same regions. As a result, the average molecular weight and crosslink density of the cured epoxy in this interphase region is probably considerably different than that of the bulk material.

B. Interphase Composition in Titanium/Epoxy Adhesive Joints

We have also used ATR to determine the structure of the interphase in titanium/epoxy adhesive joints. As described above, samples were prepared by curing epoxy beams against titanium beams and then propagating cracks very near the interface to debond the beams. The ATR spectra were then obtained by pressing the failure surface of the epoxy beam against the face of an internal reflection element.

Spectra shown in Figures 9A and 9B were obtained from the failure surfaces of epoxy beams that were cured against primed and unprimed titanium beams, respectively, using a tertiary amine salt curing curing agent and then debonded. A Ge IRE and a 60^{o} angle of incidence were used to obtain the spectra. The spectrum shown in Figure 10 was obtained by subtracting the spectrum in Figure 9B from that in Figure 9A. The strong bands near 1040 and 1130 cm^{-1} in the spectrum shown in Figure 10 are characteristic of siloxane polymers, indicating that the failure surface of the epoxy beam consisted mostly of primer and that failure occurred close to the primer/oxide interface. No bands related to unique species in the interphase were observed.

The experiment was repeated using the same Ge IRE but a smaller angle of incidence (45^{o}) to increase the depth of penetration but the results were similar. Difference spectra obtained by subtracting ATR spectra of epoxy beams debonded from primed and unprimed substrates contained only the bands near 1040 and 1130 cm^{-1} characteristic of siloxane polymers. No new bands due to unique species in the interphase were observed and it was concluded that the silane polymerized at the interface without significant interdiffusion with the epoxy.

The spectra shown in Figures 11A and 11B were obtained using a Ge IRE and a 60^{o} angle of incidence from the failure surface of an epoxy beam that was cured against primed and unprimed titanium beams, respectively, using an anhydride

curing agent with a tertiary amine accelerator and then debonded. The difference spectrum obtained by subtracting the spectrum in Figure 11B from that in Figure 11A is shown in Figure 12 and was characterized by a strong band near 1100 cm^{-1}, by weak bands near 1700, 1570, 1630, and 1780 cm^{-1}, and by a weak negative band near 1740 cm^{-1}. The bands near 1780 and 1740 cm^{-1} are related to anhydride and ester groups, respectively, while those near 1570 and 1630 cm^{-1} are related to amide groups (21). The band near 1700 cm^{-1} was attributed to imide groups.

A unique species was formed in the interphase resulting from the reaction of the γ-APS primer with the anhydride curing agent to form amide groups. Further reaction resulted in the formation of a few imide groups. The spectrum shown in Figure 12 implies that there were more anhydride and amide groups and less ester groups in the interphase of the primed joints than in the interphase of the unprimed joints. Thus, the primer decreased the rate at which the anhydride was consumed and the manner in which it was consumed.

When the depth of penetration was increased by using the Ge IRE with a smaller angle of incidence (45^{o}) or by using a KRS-5 IRE with the same angle of incidence (60^{o}), similar results were obtained. That is, there was more amide formation and unreacted anhydride and less ester formation in the interphase of epoxy beams cured on primed

titanium beams than in the interphase on unprimed titanium beams.

C. Effect of Substrate on Interphase Structure

As indicated above, ATR can be used to determine the structure of polymer interphases at depths of a few thousand angstroms into the polymer. Reflection-absorption infrared spectroscopy (RAIR) and XPS are more useful for determining the structure of interphases within a few tens of angstroms of the substrate surface. We have used RAIR and XPS to determine the effect that metal substrates have on the structure, and thus the properties, of silane primers cured against the metals.

The RAIR spectra obtained from a thin film of γ-APS deposited on an iron substrate from a 2% aqueous solution after curing at room temperature for thirty minutes and after curing at 110°C for one hour are shown in Figures 13A and 13B, respectively. The spectrum shown in Figure 13A is similar to those that have been reported previously for thin films of γ-APS formed on iron (22) and is dominated by a strong band near 1130 cm^{-1} and by moderately intense bands near 1630, 1570, 1470, 1330, and 1040 cm^{-1}. The bands near 1130 and 1040 cm^{-1} are related to siloxane polymers, indicating that γ-APS primer was hydrolyzed in solution and then polymerized on the surface of the iron substrate. Bands near 1630, 1570, 1470, and 1330 cm^{-1} are all related to amine bicarbonate salts formed by carbon dioxide and water absorbed by the primer films (23).

When the spectra shown in Figure 13 are compared, it is evident that heating the γ-APS films at 110°C had a significant effect. The band near 1130 cm^{-1} increased in frequency to about 1150 cm^{-1} and the shoulder near 1040 cm^{-1} was clearly resolved, indicating additional polymerization within the films. In addition, the bands near 1630, 1570, 1470, and 1330 cm^{-1} all decreased in intensity due to the desorption of carbon dioxide and water and to the break-up of the bicarbonates. However, it is interesting that these bands did not completely disappear. That is, once carbon dioxide was desorbed, it was reabsorbed when the γ-APS films were exposed to a humid atmosphere containing carbon dioxide.

The RAIR spectra obtained from a thin film of γ-APS deposited on a 2024 aluminum substrate after curing at room temperature for thirty minutes and after heating at 110°C for one hour are shown in Figures 14A and B, respectively. Spectra obtained from the as-formed films after curing at room temperature were similar to those formed on iron except for some subtle differences. For example, the main band related to siloxane formation was near 1100 cm^{-1} for films formed on 2024 aluminum and near 1130 cm^{-1} for films formed on iron. The second band characteristic of siloxanes was near 1040 cm^{-1} for films formed on iron but was hardly observed for films formed on aluminum. These differences indicate that the degree of polymerization was less for γ-

APS films formed on 2024 aluminum than on iron. Otherwise, the as-formed films were quite similar.

When the spectra shown in Figures 13B and 14B are compared, it is evident that drying at elevated temperatures had different effects on γ-APS films formed on 2024 aluminum and on iron. For example, heating lead to formation of a band near 1660 cm^{-1} in spectra of γ-APS on 2024 aluminum but not on iron. Moreover, γ-APS films on iron reabsorbed carbon dioxide after heating and reformed bicarbonates more readily than films formed on 2024 aluminum.

Differences in the behavior of γ-APS films on 2024 aluminum and iron were probably related to the effectiveness of the metals as catalysts for the oxidation of the amino groups. The band that appeared near 1660 cm^{-1} in the spectra of γ-APS films on 2024 aluminum after heating at 110°C for one hour was probably related to oxidation of the amino groups to form imines (24) as shown below:

$$2\ RCH_2NH_2 + O_2 > 2RCH{=}NH + 2H_2O$$

Copper present in the 2024 aluminum substrates is a powerful catalyst for such oxidation but iron is much less effective. As a result, imines formed much more readily on 2024 aluminum than on iron. However, imines may be less likely to form bicarbonates than are amines. Therefore, heat-treated films on 2024 aluminum reabsorbed carbon dioxide to a much smaller extent than heat-treated films on iron. These conclusions were supported by results obtained using copper and titanium substrates. Imines formed readily when

γ-APS films were deposited on copper substrates and then heat-treated. However, the band near 1660 cm^{-1} was not observed when γ-APS films were formed on titanium and heated, implying that imines do not form so easily on titanium and that titanium is less effective as a catalyst for the oxidation of amines than copper.

Preliminary results obtained from XPS also indicated that γ-APS films formed on 2024 aluminum are more complex than those formed on iron. The N(1s) spectra of films formed on iron consisted of a single band near 400 eV that was related to free primary amino groups but those of films formed on 2024 aluminum were much more complex and consisted of several overlapping bands (see Figure 15). One band was related to free amino groups. The others may be related to imine groups and to amino groups protonated by surface hydroxyls.

These results are extremely interesting since they show that γ-APS can undergo degradation reactions at temperatures that are commonly used in curing adhesives and matrices in composites. Degraded γ-APS will be less effective as a coupling agent or primer since half of the reactive hydrogen atoms from the amino groups are removed during the formation of imines, making the silane less likely to react with an adhesive or a matrix resin.

Considering that some metals catalyze the degradation but others do not, it is evident that the performance of γ-APS can vary significantly depending on the substrate.

However, it should be possible to reduce the effects or degradation reactions and to obtain consistent performance on a variety of substrates by curing adhesives or composites in inert atmospheres.

IV. Conclusions

The results obtained here indicate that a metal substrate can have a significant effect on the structure and thus the properties of an adhesive cured against that substrate. When an epoxy adhesive iss cured against aluminum using a polyamine curing agent, hydroxyl groups present on the oxide surface protonate the nitrogen atoms in the curing agent and catalyze the curing reaction. The result is an interphase region that has a considerably different network structure than the bulk adhesive.

The use of silane primers can result in complex interphases depending on the silane and the adhesive. When an epoxy is cured with an anhydride curing agent against a metal that has been pretreated with a primer consisting of γ-aminopropyltriethoxysilane (γ-APS), the silane and the epoxy interdiffuse and the silane reacts with the anhydride, resulting in an interphase that has a much different structure than the bulk adhesive. When the same epoxy is cured with a tertiary amine salt curing agent against a pretreated metal, the silane seems to remain near the metal surface, resulting in an interphase that is composed mostly of a siloxane polymer.

Metal surfaces can still have a significant effect on the structure of the interphase even when a silane primer is used. When γ-aminopropyltriethoxysilane (γ-APS) primers are deposited on 2024 aluminum or copper and then heated to temperatures above about 110°C, a reaction occurs in which the amino groups are oxidized to imine groups. When similar primers are deposited on iron or titanium and then heated, less oxidation of the amino groups occurs. As a result, different interphases may be expected on different metals even when the same silane primer and adhesive are used.

VI. References

1. Venables, J. D., McNamara, D. K., Chen, J. M., Sun, T. S., and R. L. Hopping, Appl. Surf. Sci. 3, 88 (1979).

2. Ahearn, J. S., Davis, G. D., Sun, T. S., and J. D. Venables, in Proc. Symp. Adhesion Aspects Polymer Coatings, K. L. Mittal, ed., Plenum Press, New York, 1983, p. 288.

3. Ditchek, B. M., Breen, K. R., Sun, T. S., and J. D. Venables, in Proc. 12th SAMPE Tech. Conf., M. Smith, ed., SAMPE, Azusa, CA, 1980, p. 882.

4. Davis, G. D., Sun, T. S., Ahearn, J. S., and J. D. Venables, J. Matls. Sci. 17, 1807 (1982).

5. Hardwick, D. A., Ahearn, J. S., and J. D. Venables, J. Matls. Sci. 19, 223 (1984).

6. Drzal, L. T., Rich, M. J., and P. F. Lloyd, J. Adhesion, 16, 1 (1982).

7. Boerio, F. J., and R. G. Dillingham, in Proc. Intl. Symp. Adhesive Joints: Formation, Characteristics, and Testing, K. L. Mittal, ed., Plenum Press, New York, 1984, p. 541.

8. Boerio, F. J., and J. W. Williams, Appl. Surf. Sci. 7, 19 (1981).

9. Boerio, F. J., and C. H. Ho, J. Adhesion, in press, 1986.

10. Davis, G. D., and J. D. Venables, to be published, 1986.

11. Boerio, F. J., Gosselin, C. A., Dillingham, R. G., and H. W. Liu, J. Adhesion 13, 159 (1981).

12. Riggs, W. M., and M. J. Parker, in Methods of Surface Analysis, A. W. Czanderna, ed., Elsevier Scientific Publishing Co., Amsterdam, 1975.

13. Dilks, A., in Electron Spectroscopy: Theory, Techniques and Applications, vol. 4, C.R. Brundle and A.D. Baker, eds., Academic Press, New York, 1981.

14. Thomas, H. R., and J.M. O'Malley, Macromolecules 12, 323 (1979).

15. Willis, H. A., and V. J. Zichy, in Polymer Surfaces, D. T. Clark and W. J. Feast, eds., John Wiley and Sons, London, 1978, ch. 15.

16. Dillingham, R. G., Ondrus, D. J., and F.J. Boerio, J. Adhesion, in press, 1986.

17. Boerio, F. J., unpublished data.

18. Ondrus, D. J., and F. J. Boerio, to be published.

19. Lee, H., and K. Neville., Handbook of Epoxy Resins, McGraw-Hill, New York, 1967.

20. B.A. Rozenburg, in Advances in Polymer Science, vol. 75, K. Dusek, ed., Springer-Verlag, Heidelberg, 1986.

21. Garton, A., J. Polymer Sci., Polym. Chem. Ed. 22, 1495 (1984).

22. Boerio, F. J., Schoenlein, L. H., and J. E. Greivenkamp, J. Appl. Polymer Sci. 22, 203 (1978).

23. Boerio, F. J., Williams, J. W., and J. M. Burkstrand, J. Colloid Interface Sci. 91, 485 (1983).

24. Sung, N. H., Kaul, A., Chin, I., and C.S.P. Sung, Poly. Eng. Sci. 22, 637 (1982).

Table 1

Atomic percentages of carbon species calculated and observed for an epoxy adhesive cured with triethylenetetraamine.

	C-C(%)	C-N(%)	C-O(%)	C=O(%)
Calculated, uncured adhesive	59.0	6.3	35.0	0.0
Calculated, cured adhesive	59.0	8.3	33.0	0.0
Observed, bulk adhesive	57.0	8.5	32.0	2.0
Observed, adhesive interphase	59.0	11.4	28.0	1.0

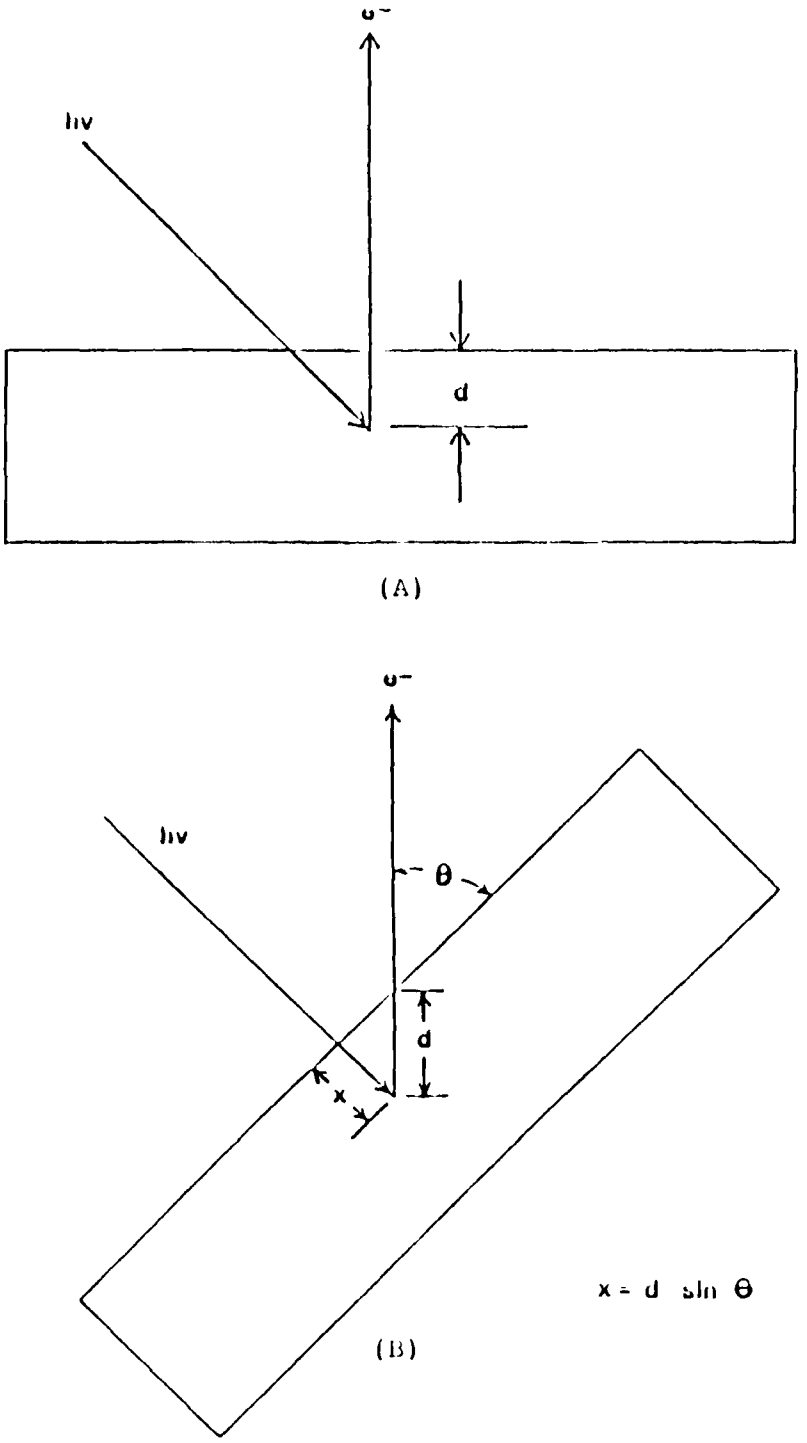

Figure 1. Depth-profiling of solid surfaces using angle-resolved XPS. In (A) the sample surface is normal to the optical axis of the energy analyzer. In (B) the sample surface makes an angle θ with the optical axis.

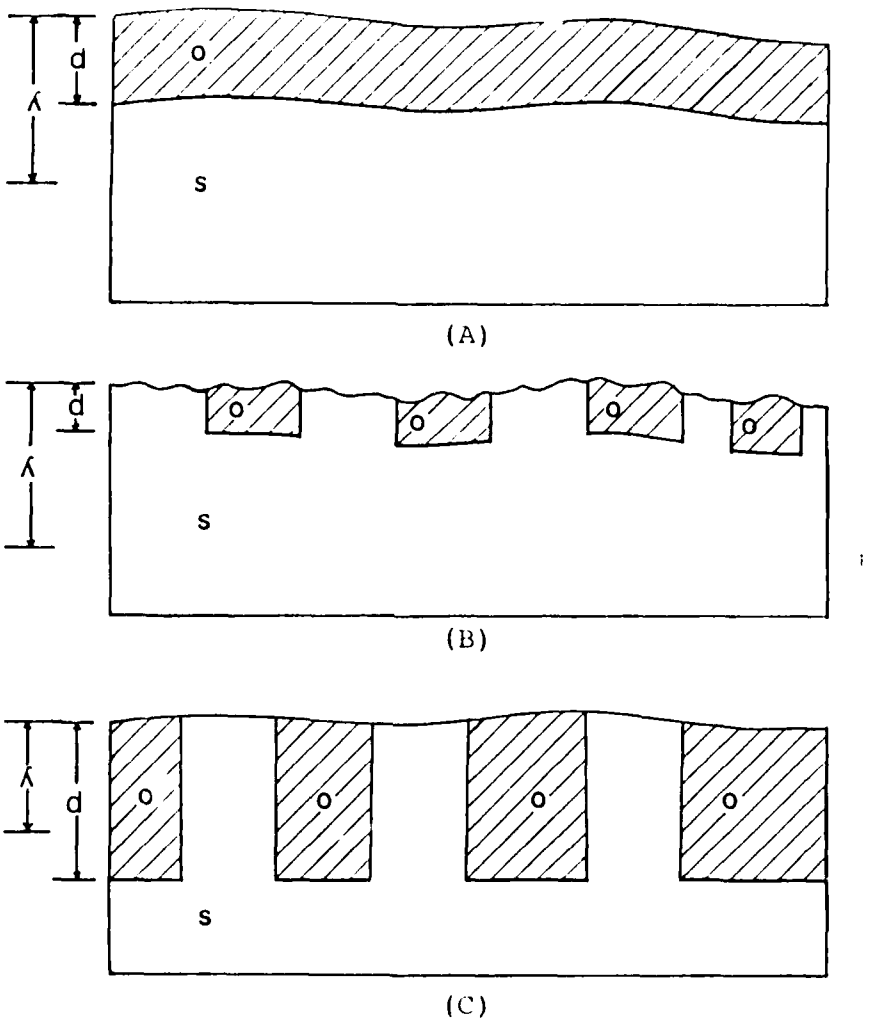

Figure 2. Three morphologies that can be identified using angle-resolved XPS. λ is the average escape depth of photoelectrons and d is the average thickness of an overlayer. In (A) there is a continuous overlayer on a substrate. In (B) there is a discontinuous overlayer with an average thickness less than the electron escape depth. In (C) there is a discontinuous overlayer with an average thickness greater than the escape depth.

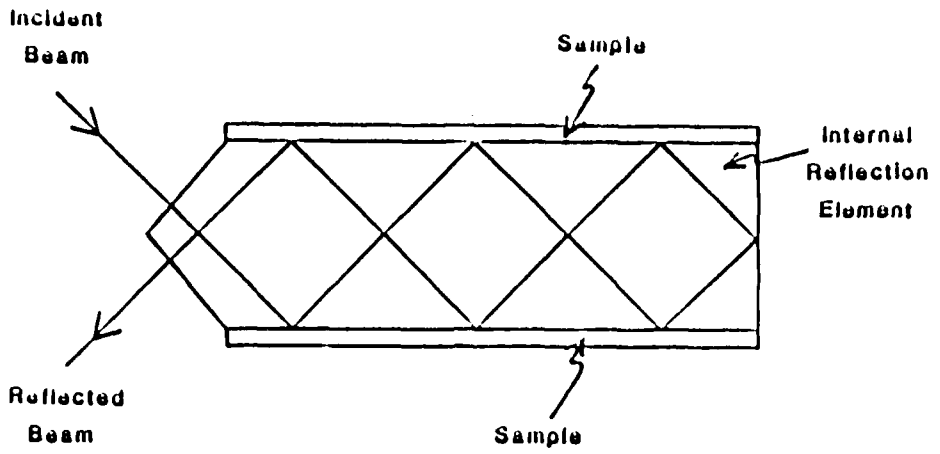

Figure 3. Experimental set-up for internal reflection infrared spectroscopy (ATR).

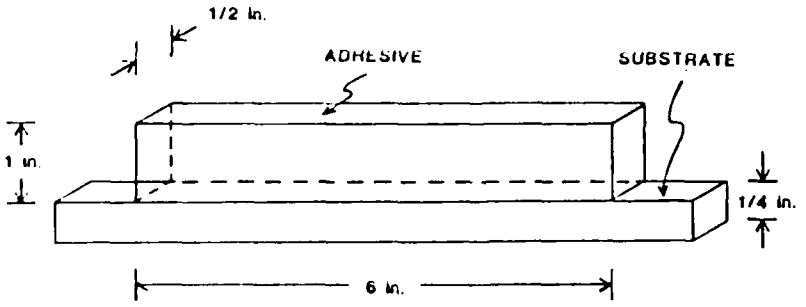

Figure 4. Double cantilever beam specimen

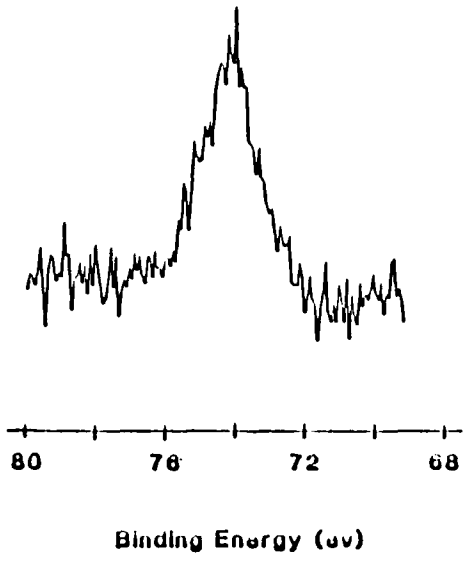

Figure 5. Al(2p) XPS spectrum from the epoxy fracture surface.

Figure 6. RAIR spectrum from the aluminum fracture surface.

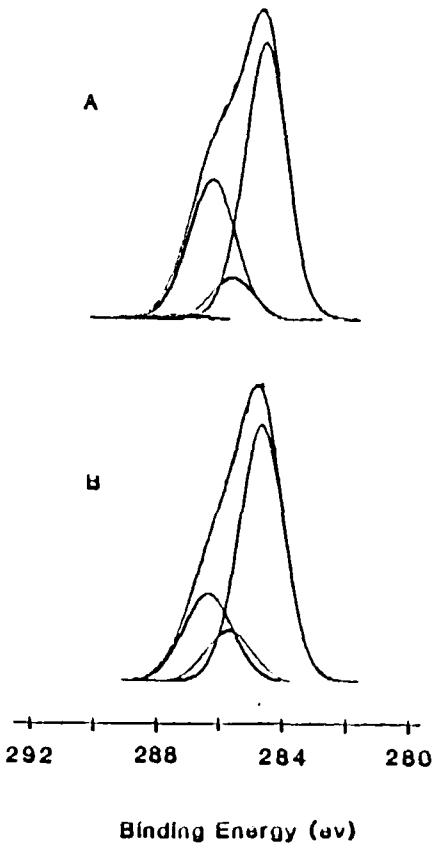

Figure 7. C(1s) XPS spectra from the (A) - bulk, cured epoxy and (B) - epoxy fracture surface.

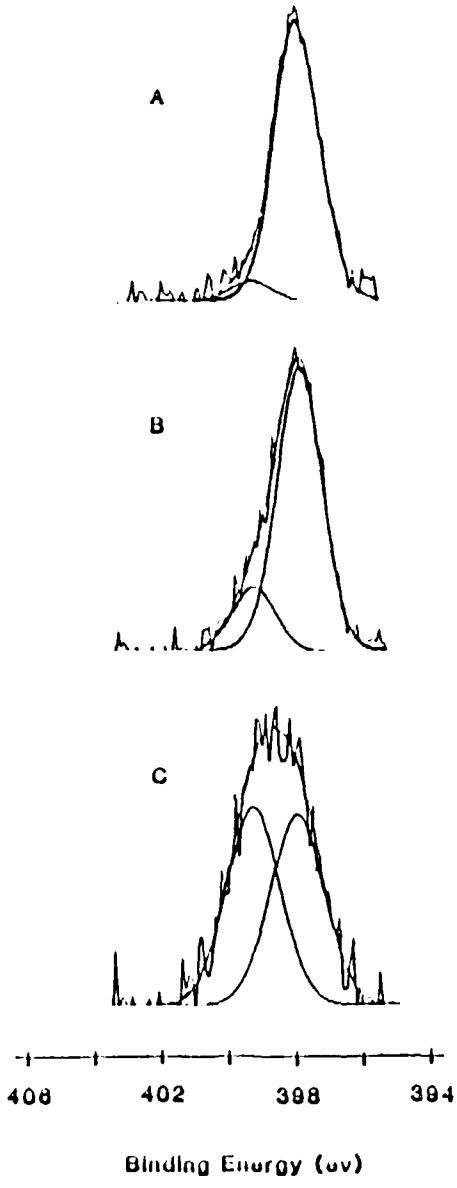

Figure 8. N(1s) XPS spectra from the (A) - bulk, cured resin, (B) - epoxy fracture surface, and (C) - aluminum fracture surface.

(A)

(B)

Figure 9. ATR infrared spectra from epoxy/tertiary amine adhesives cured against titanium beams that were (A) - primed with a 2% aqueous solution of γ-APS and (B) - unprimed.

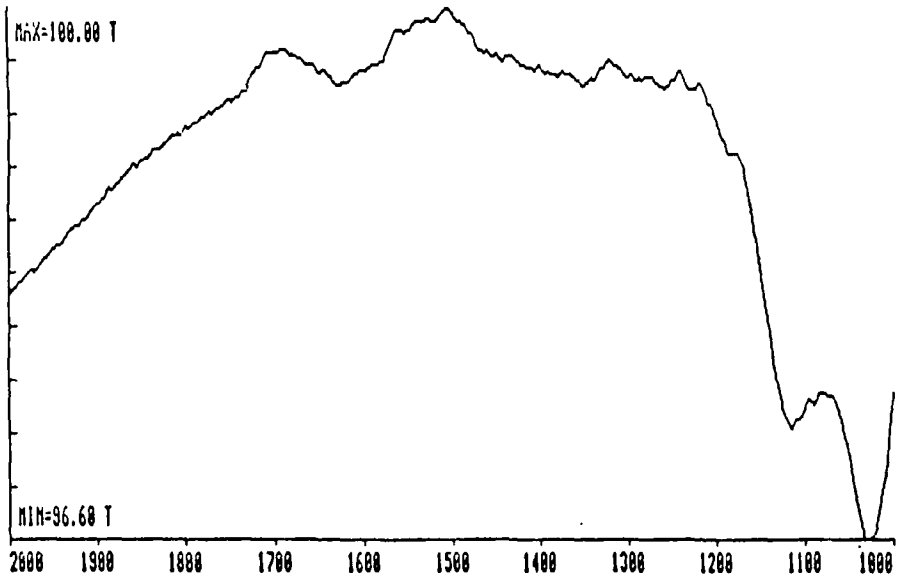

Figure 10. Difference spectrum showing bands due to silane primer near 1040 and 1120 cm^{-1}.

(A)

(B)

Figure 11. ATR infrared spectra from epoxy/anhydride adhesives cured against titanium beams that were (A) - primed with a 2% aqueous solution of γ-APS and (B) - unprimed.

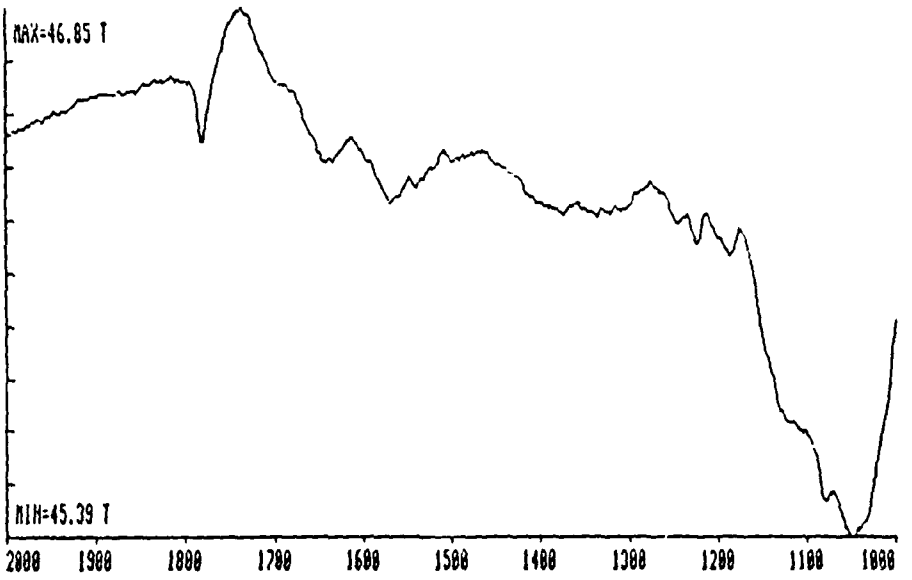

Figure 12. Difference spectrum showing bands due to amide (1580 and 1640 cm^{-1}) and imide (1700 cm^{-1}) formation and to residual anhydride (1785 cm^{-1}) in the interphase.

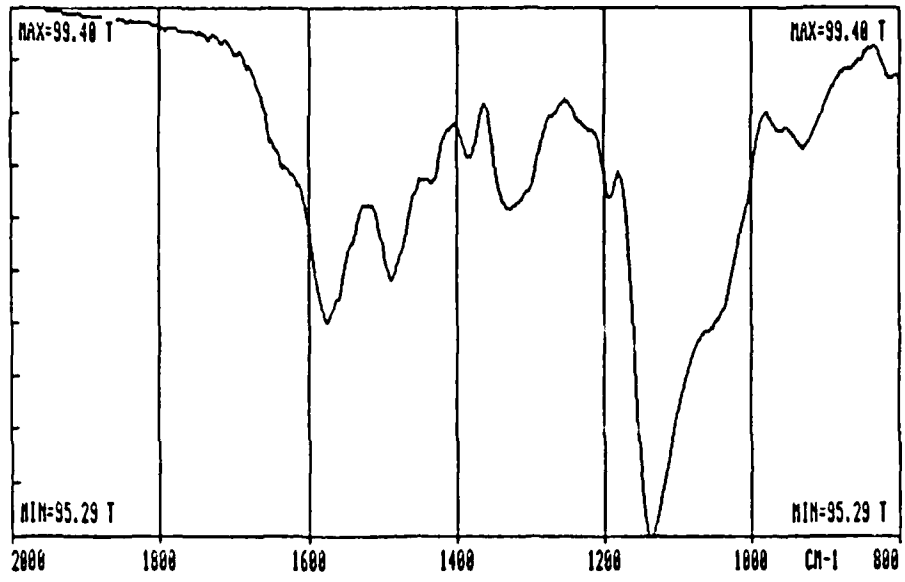

(A)

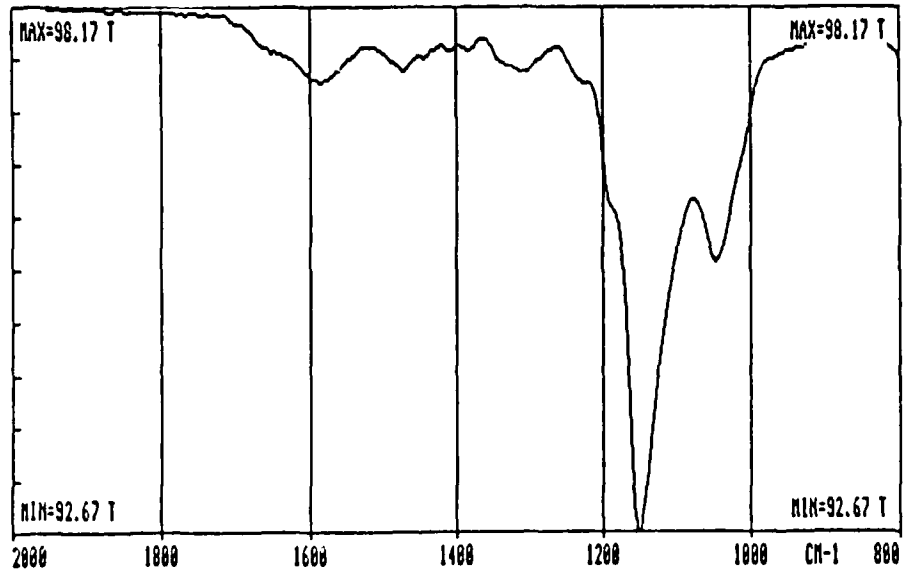

(B)

Figure 13. RAIR infrared spectra obtained from polished steel dipped into a 2% aqueous solution of γ-APS for 1 minute and then blown dry with N_2: (A) - after curing for 30 minutes at room temperature and (B) - after post curing for 1 hour at 110°C.

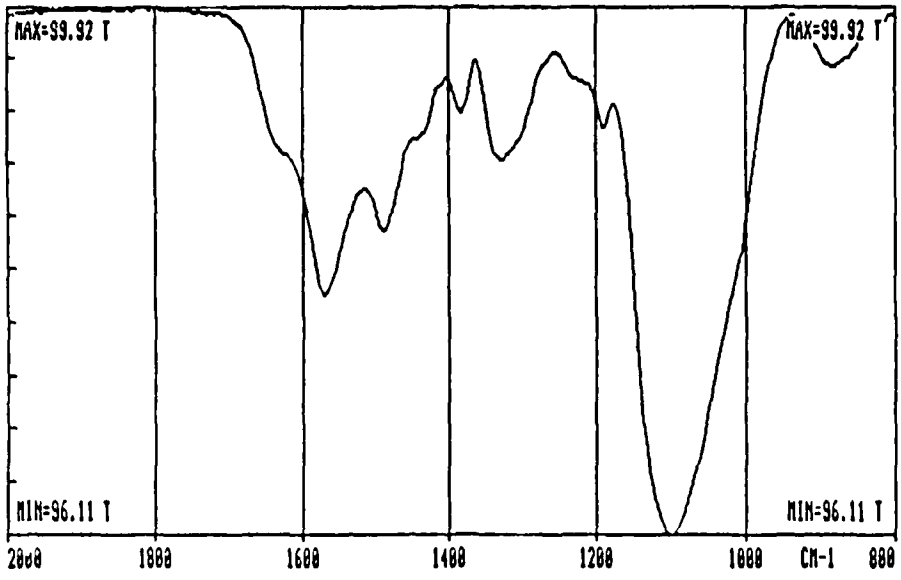

(A)

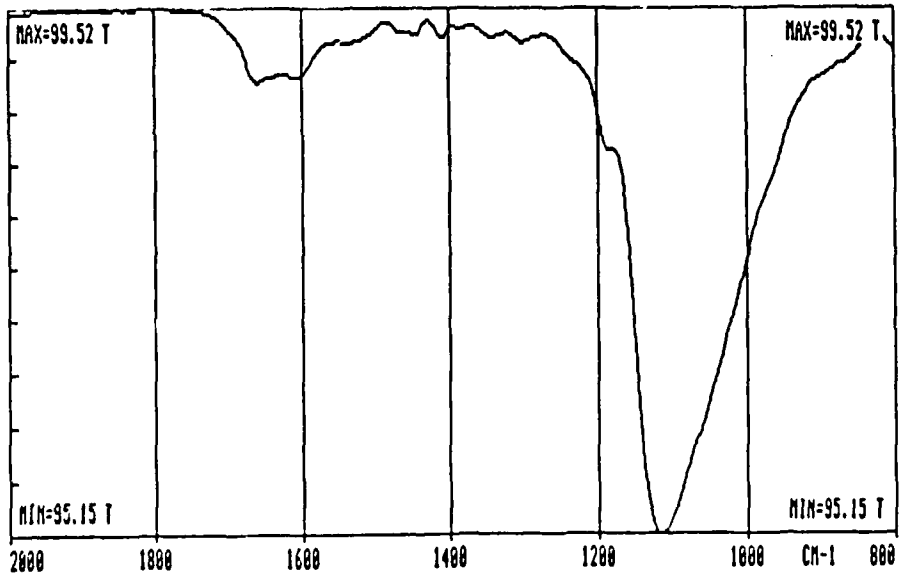

(B)

Figure 14. RAIR infrared spectra obtained from polished 2024 aluminum dipped into a 2% aqueous solution of γ-APS for 1 minute and then blown dry with N_2: (A) - after curing for 30 minutes at room temperature and (B) - after post curing for 1 hour at 110°C.

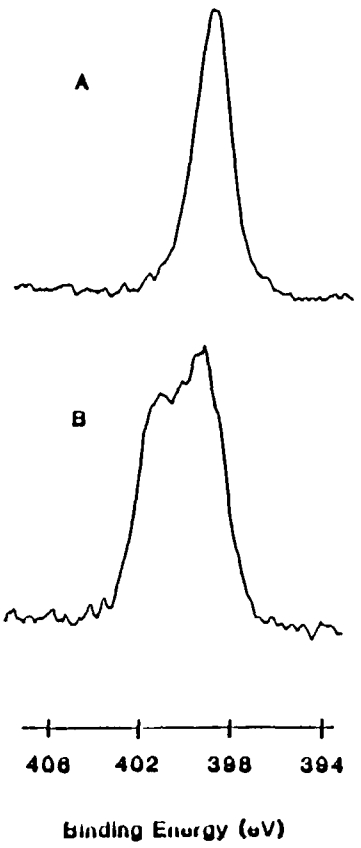

Figure 15. N(1s) spectra obtained from γ-APS films deposited on (A)- iron and (B) - aluminum substrates from 2% aqueous solutions and dried at room temperature for 30 minutes.

ONR Adhesion Science Distribution List

Dr. R. C. Pohanka
Code 1131
800 North Quincy Street
Arlington, VA 22217

Defense Technical Information Center (12 cys)
Building 5, Cameron Station
Alexandria, VA 22314

Dr. L. H. Peebles, Jr.
Office of Naval Research
Code 1131
800 North Quincy Street
Arlington, VA 22217

Office of Naval Research
Code 1113 (Attn: Dr. K. J. Wynne)
800 North Quincy Street
Arlington, VA 22217

Office of Naval Research
Code 1132 (Attn: Dr. R. S. Miller)
800 North Quincy Street
Arlington, VA 22217

AFOSR
Attn: Dr. D. R. Ulrich, Building 410
Bolling AFB
Washington, DC 20332

Naval Research Laboratory
Code 6120 (Attn: Dr. W. B. Moniz)
4555 Overlook Avenue, SW
Washington, DC 20375

NADC
Code 6063
Attn: S. Brown
R. Trabacco
Warminster, PA 18974

NAVSEA 109CM4
Attn: Mr. C. Zanis
Washington, DC 20362

Naval Air Systems Command
440-JP1 (Attn: Dr. G. Heiche)
Washington, DC 20361

AFWAL/MLBM (T. E. Helminiak)
WPAFB, OH 45433

AFWAL/MLBM (I. J. Goldfarb)
WPAFB, OH 45433

AFWAL/MLBM (R. Van Deusen)
WPAFB, OH 45433

NSWC
Attn: Dr. J. Augl
White Oak Laboratory
Silver Spring, MD 20910

NBS
Polymer Science & Studies Division
Attn: Dr. D. L. Hunston
Washington, DC 20234

Army Research Office
Attn: Dr. R. Reeber
P.O. Box 12211
Research Triangle Park, NC 27709

NASA
Attn: T. L. St.Clair MS226
S. Johnson MS188E
Langley Research Center
Hampton, VA 23665

AMMRC
Attn: Dr. S. E. Wentworth
Watertown, MA 02172

Dr. S. Thornton
Texas Research Institute
9063 Bee Caves Road
Austin, TX 78746

Naval Research Laboratory
Code 8433 (Attn: Dr. I. Wolock)
4555 Overlook Avenue, SW
Washington, DC 20037

Naval Weapons Center
Attn: Mr. A. Amster
China Lake, CA 93555

Professor S. Wang
Dept. of Theoretical & Applied Mechanics
University of Illinois
Urbana, IL 61801

Dr. J. D. Venables
Martin Marietta Laboratories
1450 South Rolling Road
Baltimore, MD 21227

Dr. R. W. Seibolt
Hughes Aircraft Co.
Bldg E4 MS F150
P.O. Box 902
El Segundo, CA 90245

Prof. H. F. Brinson
Prof. T. Ward
Prof. J. P. Wightman
Prof. J. N. Reddy
Prof. D. A. Dillard
Center for Adhesion Science
VPI
Blacksburg, VA 24060

Prof. A. N. Gent
Institute of Polymer Science
University of Akron
Akron, OH

Professor H. Ishida
Dept. of Macromolcular Science
Case Western Reserve University
Cleveland, OH 44106

Professor F. J. Boerio
Dept. of Materials Science
University of Cincinnati
Cincinnati, OH 45221

Dr. J. Ahearn
Martin Marietta Laboratories
1450 South Rolling Road
Baltimore, MD 21227

NRL/USRD
Attn: Dr. R. W. Timme
Orlando, FL 32806

END

3-87

DTIC